2017

Expression of FAM171B Protein in Mouse Brain Tissue

Quan Tran
Minnesota State University, Mankato

Expression of FAM171B Protein in Mouse Brain Tissue.

By
Quan Tran

A Thesis Submitted In Partial Fulfillment of the
Requirements for the Degree of
Master of Science
In
Biological Sciences

Minnesota State University, Mankato
Mankato, Minnesota
December 4th, 2017

12/4/2017

Expression of FAM171B Protein in Mouse Brain Tissue.

Quan Tran

This Thesis has been examined and approved by the following members of the student's committee.

Dr. Geoffrey Goellner
Advisor

Dr. David Sharlin
Committee Member

Dr. Rachel Cohen
Committee Member

Table of Contents

Abstract

Expression of FAM171B Protein in Mouse Brain Tissue

Name - Quan Tran

Degree – Master of Science in Biology

University - Minnesota State University Mankato MN56001

Year - 2017

Polyglutamine (polyQ) diseases are inherited fatal neurodegenerative disorders caused by expansion of trinucleotide cytosine-adenine-guanine (CAG) repeats, encoding abnormally long glutamine tracts in respective disease proteins. Currently, there are nine polyQ diseases- including Huntington's disease and a number of Spinocerebellar ataxias. Interestingly, expanded polyQ proteins are prone to aggregate, and this aggregation may underlie neurodegeneration. In this study, we investigate the expression and localization of FAM171B (a novel polyQ protein) in the brain. Western blotting reveals that FAM171B protein is indeed expressed in the developing and adult mouse brain. Furthermore, immunohistochemical analyses suggests widespread localization of FAM171B to many brain regions - with pronounced expression in the hippocampus, cerebellar Purkinje cells, and cerebral cortex. As a novel polyQ protein that is expressed in the brain, our observations suggest that FAM171B can be considered a candidate gene for as yet molecularly uncharacterized neurodegenerative diseases.

Acknowledgements

I would like to express my deepest gratitude to my advisor and mentor Dr.Geoffrey Goellner for his support, guidance and encouragement during the course of my Master program. I am grateful for his expert advice and critical suggestions that help me through this rigorous research. Thank you for your constant support, and believe in me. I would also like to extend my gratitude to my committee members Dr. David Sharlin, and Dr. Rachel Cohen for their contributions to my research and invaluable input and suggestion. I would also like to offer my earnest thanks to the entire lab mates and the administrative staff of the department of Biological science for their assistance and support.

Introduction

A large number of severe neurodegenerative diseases, including: Huntington's disease (HD), spinal-bulbar muscular atrophy (SBMA), several spinocerebellar ataxias (SCAs) and Dentatorubral-Pallidoluysian atrophy (DRPLA), result from an expansion mutation of a trinucleotide cytosine-adenine-guanine (CAG) repeat in the human genome (Table 1).

Table 1. Summary of Polyglutamine diseases (Hueng, 2014).

Disease	Pattern of Inheritance	Normal Repeat length	Disease Repeat length	Affected Brain Region
Spinobulbar Muscular Atrophy	X-linked recessive	9-36	36-62	Anterior horn, bulbar neurons and dorsal root ganglia
Huntington disease	Autosomal dominant	6-35	36-121	Striatum and cerebral cortex
Dentatorubral Pallidoluysian Atrophy	Autosomal dominant	3-38	49-88	Cerebellum, cerebral cortex and basal ganglia
Spinocerebellar ataxia type 1	Autosomal dominant	6-39	41-83	Cerebellar, Purkinje cells brain stem
Spinocerebellar ataxia type 2	Autosomal dominant	14-32	34-77	Cerebellar, Purkinje cells brain stem
Spinocerebellar ataxia type 3	Autosomal dominant	12-40	62-86	Cerebellar dentate neurons, basal ganglia and brain stem
Spinocerebellar ataxia type 6	Autosomal dominant	4-18	21-30	Cerebellar Purkinje cells dentate nucleus and inferior olive
Spinocerebellar ataxia type 7	Autosomal dominant	7-18	38-200	Cerebellum, brain stem
Spinocerebellar ataxia type 17	Autosomal dominant	25-43	45-63	Cerebellar, Purkinje cells, inferior olive

As CAG encodes for the amino acid glutamine (Q), aberrant proteins containing polyQ stretches that expand beyond their normal polymorphic range cause the above diseases, which are referred to collectively as polyQ diseases (Zoghbi and Orr 2000).

CAG triplet repeat expansion mutation was first described in 1991 as a mutation in the androgen receptor gene causing the progressive motor neuron disease SBMA (La Spada et al., 1991). Since then, eight other diseases have also been described as being derived from a CAG repeat expansion that passes beyond a specific length threshold. PolyQ diseases are inherited in an autosomal dominant fashion, with the exception of spinobulbar muscular atrophy, and typically are quite rare (Margulis, 2013). Of the polyQ diseases, HD and SCA3 have the highest prevalence rates affecting ~1:10,000 individuals worldwide (Margulis, 2013) and (Bauer, 2013). Although polyQ diseases are rare, they are devastating to affected individuals as well as their families. To date, polyQ disease therapy remains a significant challenge (Xia, 2004). Therefore, understanding both polyQ pathogenesis and the normal molecular function of wild-type polyQ proteins within cells may help find treatments or even cures for polyQ disease.

The pathological hallmark of polyQ disease is the accumulation of intracellular inclusions or aggregates in widespread central nervous system and peripheral tissues (Bradford, 2010). Interestingly, each disease pathology is largely restricted to specific brain areas (Table 1) (Sharp *et al*., 1995). Intranuclear inclusions are commonly found in degenerating neurons of the cerebral cortex, cerebellar Purkinje cells, cerebellum, brain stem and spinal tract (Zoghbi, 1999).

Numerous studies of affected neurons reveal that polyQ toxicity is likely due to the ability of expanded polyQ peptides to form these inclusions (Ross and Poirer, 2004). Indeed, aggregate formation likely explains the "toxic gain-of-function" that occurs with expanded polyQ tracts. Misfolded and aggregated mutant polyQ proteins may affect global cellular gene expression profiles, disrupt nuclear organization, or inhibit proteasomal function (Williams and Paulson, 2008; Hueng, 2014, Goellner and Rechsteiner 2003). Although numerous studies have shown that mutant polyQ proteins form insoluble inclusions, there is no definitive agreement as to whether neuronal aggregates play an essential role in pathogenesis. Indeed, some studies even suggest that expanded polyQ protein aggregates may actually protect from cytotoxicity (Paulson et al., 1997; Haacke *et al.,* 2006; Saudou, 1998; Huynh, 2000; Tarlac, 2007).

Significant evidence from both cellular and animal models suggests that peptide fragments of the expanded polyQ protein may actually be more toxic than their full-length counterparts (Duennwald *et al*., 2006; Ikeda *et al*., 1996). For example, when a fragment of mutant ataxin-3 was expressed in a mouse model of SCA3, the fragment induced apoptotic cell death more rapidly than mice expressing the full-length mutant ataxin-3 (Ikeda *et al*., 1996). Thus, protein fragments containing expanded polyQ tracts seem to be more toxic than full-length proteins, and this may be a clue regarding the pathogenic process.

Interestingly, a number of expanded polyQ proteins seem to localize to the nucleus where they may abnormally interact with transcription factors to affect gene expression profiles. For example, Yoo et al. (2003) demonstrated that expanded CAG

repeats introduced into the mouse *sca7* gene resulted in substantial disruption of photoreceptor gene expression. In another study, mutant ataxin-1 was found to interact with PQBP-1, and this association was linked to decreased transcriptional levels in Spinocerebellar type I (Komuro *et al.,* 1999). Studies in Huntington's disease have also revealed that expanded polyQ tracts interfere with CBP-activated gene expression, and over expression of CBP rescues polyQ toxicity (Nucifora *et al.,* 2001). Thus, numerous studies have linked expanded polyQ tracts to gene expression dysregulation. However, the precise mechanisms leading to downstream neuronal cell death are not entirely clear.

One feature common to the majority of polyQ disease is late onset. In affected individuals, polyQ diseases typically manifest in the fourth and fifth decade of life. Interestingly, however, the precise age of onset and severity of disease is dependent upon the severity of CAG repeat tract expansion. Normal alleles of polyQ disease linked genes are typically polymorphic- containing between 10-30 CAG repeats (Table 1), while mutant alleles contain 40-100's of repeats (Agnieszka and Wlodzimierz, 2014). Interestingly, there seems to be a strong correlation between disease severity and mutant repeat tract length. In general, the longer the mutant repeat tract the earlier and more severely each disease manifests in afflicted individuals (Walker, 2007). Furthermore, disease symptoms often appear earlier in subsequent generations within affected polyQ families. This phenomenon of genetic anticipation can be molecularly explained by the increased genetic instability that accompanies increased CAG tract length. In other words, when a CAG repeat tract becomes long enough to cause disease, it also somehow becomes prone to more frequent DNA expansion mutations (Gacy *et al.,* 1995, Kovtun *et*

al., 2001). In general, repeat tract length changes likely occur during meiosis, and are often greater in spermatogenesis than oogenesis (La Spada *et al.,* 1992).

The mechanism underlying the abnormal expansion of polyQ stretches remains largely unknown. However, formation of alternative DNA structures (such as hairpins) during meiotic replication may be fundamental to this form of genetic instability (Gacy *et al.,* 1995, Kovtun *et al.,* 2001). Indeed, the propensity for triplet repeat expansion mutation likely depends upon several factors including length of the initial triplet tract, the ability to form alternative DNA structures, and the effect of modifying genes (Zühlke, 1993, McMurray 2010).

One candidate set of modifying genes include DNA mismatch repair (MMR) enzymes. Studies have shown that, unlike hereditary forms of colon cancer, DNA mismatch repair enzymes themselves are not mutant in polyQ disease (Goellner *et al.,* 1997). Instead, the evidence suggests that normal DNA repair machinery is "hijacked" by expanded triplet repeat tracts (perhaps by alternative DNA structure formation), and while trying to fix this DNA structural abnormality repair enzymes may instead actually contribute to the mutation (Manley *et al.,* 1999; Kovtun and McMurray, 2001). In support of this idea, when HD transgenic mice were crossed with mice lacking MSH2, triplet repeat expansion in germ cells and somatic tissue was abolished (Manley et al. 1999). These results suggest that MSH2 mismatch repair enzymes are somehow involved in expansion mutation, and it is likely that alternative DNA structure formation by the triplet repeats is recruiting repair enzymes to the process (McMurray, 2008).

Despite polyQ diseases sharing similar mutation and clinical features, the diseases are a complex group of disorders. Studies on proteins containing polyQ expansions continue to progress and advance, and finding better treatment options for polyQ disease remains paramount. The vast body of knowledge already contributed to polyQ disease research opens up new challenges and opportunities for greater understanding of polyQ disease. Similarly, discovery of novel proteins containing polyQ repeats with the potential to undergo expansion mutation may shed light on genetically uncharacterized neurodegenerative diseases, and elucidate the field in general.

In this regard, the sequencing of the human genome has revealed a number of completely novel proteins containing polyQ repeats that have yet to be molecularly characterized. Using the bioinformatic algorithm BLAST, our lab has recently identified one such protein FAM171B; a novel polyQ protein with approximately fourteen consecutive glutamines in its reported primary amino acid sequence (The UniProt Consortium, 2017). Further analysis reveals that FAM171B is located on chromosome 2.q31, and there are likely eight exons that can be transcribed into two predicted alternative mRNA splice forms encoding proteins of 92kDa and 48kDa respectively (The UniProt Consortium, 2017). Bioinformatic analysis suggests that FAM171B may also have various posttranslational modifications (Ex. Glycosylation) that ultimately affect its structure and function (Table 2).

Table 2. Amino acid modifications. Summary of putative posttranslational modification from human and mouse (The UniProt Consortium, 2017).

Feature Key	Position (s)	Description
Glycosylation (Human)	108	N-linked (GlcNac..) Asparagine
Glycosylation (Human)	113	N-linked (GlcNac..) Asparagine
Glycosylation (Human)	213	N-linked (GlcNac..) Asparagine
Glycosylation (Human)	268	N-linked (GlcNac..) Asparagine
Modified residue (Human)	794	Phosphoserine
Glycosylation (Mouse)	109	N-linked (GlcNac..) Asparagine
Glycosylation (Mouse)	114	N-linked (GlcNac..) Asparagine
Glycosylation (Mouse)	214	N-linked (GlcNac..) Asparagine
Modified residue (Mouse)	792	Phosphoserine

As a completely uncharacterized protein, FAM171B expression levels, tissue localization, and specific cellular functions have yet to be determined.

In this study, we perform both immunoblot and immunohistochemical assays to analyze FAM171B expression and localization within the mouse brain. Our results corroborate previous studies from our lab (that used *in-situ* hybridization), and strongly suggest that FAM171B is widely expressed throughout the brain with pronounced expression in cells of the hippocampus, cortex, and cerebellum. As we find that FAM171B is indeed expressed in the brain, this novel protein should be considered a candidate gene for as yet molecularly uncharacterized neurodegenerative diseases.

Materials and methods

Animals: C57BL/6 male mouse (IACUC 15-02) were maintained in 12.88x7.50x5.63 inch cages. Trained animal care staff provided daily monitoring of the mice. A 12:12-hour light and dark cycle was provided (0800:2000), and temperature was maintained within standard guidelines. Mice received water and certified laboratory diet (Rodent Diet, LabDiet), and were transferred to cages with clean bedding once every week. Date at which pups were born was recorded, and mice were maintained as above until they were of appropriate research age.

Mouse brain dissection: Male mice brains were dissected at postnatal days seven (P7), twenty-one (P21), and forty-two (P42), as well as six months (6M) and snap frozen by placing on dry ice. For specific brain regions study, certain brain regions (including: hippocampus, cortex, cerebellum, brain stem, and thalamus) were first isolated prior to freezing. To isolate different regions, a freshly collected brain was place on an ice-chilled slide and bisected along the midline with a razor blade. A coronal cut was made at the lower back of the brain to remove the cerebellum and brain stem. Next two spatulas were used to separate the cerebellum from the brain stem. A mid-sagittal cut was then made before left and right hippocampal regions were isolated; one spatula was anchored over the cortex, at the same time the other spatula tip was placed near the junction to allow the thalamus region to be peeled away exposing the hippocampus. While anchoring the brain with one spatula tip, the other was placed just under the caudal tip of the hippocampus and carefully applied pressure was directed to the medial white matter tracts with the anchoring spatula while moving the second spatula tip anteriorly and posteriorly. Once

the thalamus and hippocampus was removed, the remaining tissue was considered cortex. Isolated brain regions were snap frozen on dry ice and stored at – 80^{o}C for later use.

Preparation of mouse brain lysate: Whole mouse brains (and isolated brain regions described above) were weighed, thawed, and diced into fine pieces with a razor blade prior to being transferred to a microcentrifuge tube containing ice-cold 2X RIPA lysis buffer (10mM Tris pH 7.5, 300mM NaCl, 2% Nonidet P-40, 1% Na-Deoxycholate, protease inhibitor cocktail). For every one-gram of mouse brain tissue, 3ml ice-cold RIPA lysis buffer was added. Next, the mouse brain tissue solution was vigorously vortexed until homogenous, and the solution was incubated on ice for 30 minutes with occasional vortexing. Brain tissues debris was removed by microcentrifugation for 20 minutes at 18,000xg in 4^{o}C. The supernatant was aliquoted into a fresh microfuge tube, and incubated on ice prior to protein concentration determination via a Bradford assay.

Bradford assay for protein concentration: 20µl of brain lysate diluted in double deionized water (1:50, 1:100) was added to a cuvette containing 1ml Bradford reagent. The mixture was incubated for 10 minutes prior to analysis by using a spectrophotometer (nanodrop2000, Thermofisher) at 595nm absorbance. Once protein concentration was determined, an equal amount of brain lysate and 2X SDS loading buffer (1.0M Tris/HCL pH 6.8, 20% SDS, 50% Glycerol, 0.16M Dithiothreitol, 0.2mg/ml Bromophenol blue) were mixed together in a microcentrifuge tube and stored at -20^{o}C.

Western Blot: Electrophoreses of the mouse brain lysates was performed to assay for the presence of FAM171B. Briefly, 5µl molecular weight ladder (928-4000, Odyssey) and 100µg of total protein from P7, P21, P42, and 6M (as well as brain regions described

above) were loaded onto 8% SDS/PAGE gels. Electrophoreses was performed at 100 volts for 1 hour in running buffer (25mM Tris-base, 192mM Glycine, 3.5mM SDS) Next, proteins were transferred onto a nitrocellulose membrane in order to probe for FAM171B. A wet transfer system (Biorad) was utilized, and the chamber was filled with transfer buffer (2.5mM Tris-base, 19.2mM Glycine, 10%MeOH) The transfer was allowed to run over night at 100mA.

Immunoblot analysis of FAM171B protein: Nitrocellulose membranes containing mouse brain proteins were blocked in 3ml phosphate buffer solution (PBS) (Odyssey, Licor) for 3 hours at room temperature. Next, the nitrocellulose membranes were probed with 3ml primary Ab (1:1000, NBP1-93847, Novus Biological) diluted in PBS buffer, and incubated overnight at 4^{o}C. The next day, membranes were washed in Tris-buffered saline Tween (TBS-T) (25mM Tris-base, 150mM NaCl, 0.1% Tween20, pH 7.4) five times each time for five minutes. Next, 3ml of secondary antibodies (1:10,000 Goat-anti-Rabbit-IRdye680LT, Odyssey, Licor) diluted in PBS block buffer was added to the membranes and incubated overnight at 4^{o}C. The following day, membranes were washed five times in TBS-T (each time for five minutes) before imaging on a Li-COR Odyssey in the 700nm channel. Lastly, the immunoblot photographs were converted into gray scale and inverted using Adobe Photoshop.

Peptide Block Negative Control FAM171B Immunoblots: In order to verify primary Ab specificity, “peptide block” control experiments were performed. Briefly, the peptide that the Novus Ab was raised against (NBP1-93847PEP, Novus) was diluted into PBS blocking solution to yield (0.1μg/μl). In a different tube, primary Ab was diluted

(1:1000) in PBS blocking buffer, and divided into two identical aliquots. One aliquot remained unchallenged while the other received peptide (at a 2:1 molar ratio of peptide to Ab), and both antibody solutions were incubated overnight at 4^0C. The next day, both aliquots were centrifuged for 15 min at 15,000xg to pellet any immune complexes. The supernatant was then pipetted into a fresh tube to be used as an immunoblot working solution.

FAM171B Positive Control Immunoblots: HEK-293 cell lines transfected with FAM171B-GFP were used as a positive control for Ab specificity. Briefly, HEK cells were subcultured into six-well plates containing 2ml DMEM/well (Thermoscientific) culture media supplemented with 10% fetal bovine serum. Cells were allowed to attach and grow at 37^oC overnight. The next day, media from cells to be transfected was replaced with 2mL of serum free medium Opti-MEM I (GIBCO) (untransfected cells remained in original media). Cells were transfected with 500ul Opti-MEM I supplemented with 10μL lipofectamine 2000 (Invitrogen) and 5μg FAM171B- GFP plasmid. Transfection was allowed to continue at 37^oC for 4-5 hours, after which the transfection media was replaced with 2ml DMEM/Serum and the cells were incubated overnight at 37^0C. Both untransfected and transfected HEK cells were lysed with 250ml of 2X RIPA buffer/well (supplemented with protease inhibitor cocktail) and cell extracts were collected for protein concentration as above.

Immunoblot quantification of FAM171B. Immunoreactive bands were analyzed by image studio (version 3.1). All immunoreactive bands present in each lane were

measured for total protein quantification. In addition, predominant bands were measure independently, by manually selecting each band across all ages.

Immunohistochemistry tissue processing and preservation: Sagittal sections of the left hemisphere were cryo-sectioned at 20μm and collected onto "super frost charged" glass slides (Thermofisher). Briefly, we discarded the initial 200μm of brain tissue and collected the next 20μm tissue section onto the slide. Then, we discarded the next 100μm brain tissue before collecting the next 20μm section. Collected sections used for controls were adjacent to that of the experimental tissue. We repeated the above steps throughout the entire left-brain, and tissue sections were stored at -80^{o}C until IHC was performed.

Immunohistochemical procedure for frozen sections: Immunohistochemistry (IHC) was performed on frozen brain tissue as follows. Slides containing frozen sections were thawed at room temperature for 15 minutes, and then incubated in ice-cold 0.75% H_2O_2/methanol for 30 minutes to block endogenous peroxidase activity. After 30 minutes, excess fluid on the slides was tapped off on a paper towel before washing the slides with vectastain buffer (10mM Na_2PO_4, 0.9% saline (PBS), pH 7.5). Next, a blocking pen was used to mark the perimeter, and 300μl vectastain block serum (Vectastain ABC kit) was pipetted onto the slides. Slides were incubated in block serum for 2 hours at room temperature. After 2 hours, block serum was removed and 300μl of primary Ab (Rabbit anti-FAM171B, Novus) diluted 1:500 in vectastain block serum was pipetted onto the slides, and incubated at 4^{0}C overnight. Following overnight incubation, slides were washed five times (5 min each time) with vectastain buffer. Then 300μl of secondary Ab (Goat-anti-rabbit, Vectastain ABC kit) diluted 1:10,000 in vectastain block

serum was applied to each slide for 90 minutes at room temperature. Next, slides were washed as above prior to incubation in 300µl of ABC Vectastain reagent (Vectastain ABC kit) for 45 minutes. After 45 minutes, the slides were again washed five times (5 min each time) with vectastain buffer. DAB solution was then pipetted onto each slide and allowed to incubate for ~20 seconds before the slides were submersed in distilled water to stop the colorimetric reaction. Finally, slides were cover-slipped using aqua-polymount (Polyscience Inc.).

The same IHC procedure was utilized on control sections, except that the negative control sections never received primary Ab, but instead remained in vectastain block serum. Additionally, slides were exposed to a peptide block at a molar ratio of 15:1, where the primary Ab (1:500) was incubated with peptide specific for the antibody in PBS overnight at 4^0C before being applied to slides. Buffer used for Ab incubations was also changed to PBS.

Photography: We photographed brain profiles from thin DAB stained sections using optical microscope (Zeiss) with a progress C10 Plus camera (Jenoptic) connected to a computer. Photographs were taken with various objectives including: 5X (EC Plan-Neofluor, Zeiss), 40X (EC Plan-Neofluor, Zeiss), and 100X 1.25 oil (Anchroplan). Sections lengths were measured with a reticule that is divided into 0.1mm and the last 0.2mm is divided into units of 0.01mm (Krabbenhoft). Whole brain cross sections were measured using a ruler (Fine science tools), with a scale of 1mm.

Qualitative analysis: FAM171B immunostain levels (hippocampus, cerebellum, cortex, amygdala, thalamus, caudate and corpus callosum) was observed using a

compound light microscope. Relative immunostain intensity was assigned as follows: high signal (+++), medium signal (++), low signal (+), and no signal (-).

Statistical analysis: Statistically significant differences between age groups was determined by univariate ANOVA analyses using IBM SPSS statistics. All analyses measured FAM171B expression across all ages (N=3). Standard errors were calculated by using Microsoft excel.

Results

Immunoblotting of adult mouse brain extracts reveals two predominant bands at approximately 92 kDa and 48kDa, matching well the predicted molecular weights for the two FAM171B mRNA spliceforms (Figure 1). These results strongly suggest that FAM171B is indeed expressed in mouse brain.

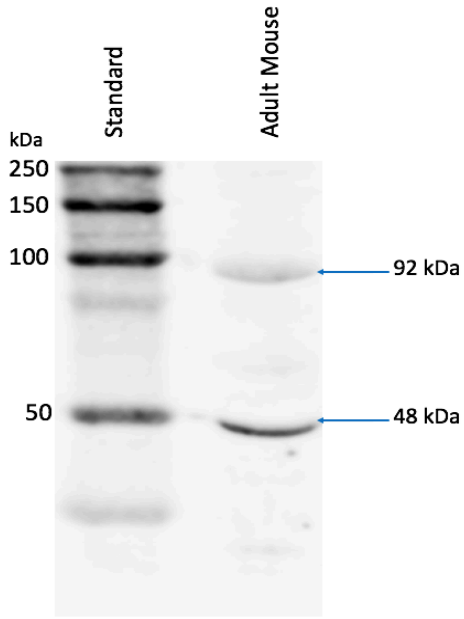

Figure 1. FAM171B protein is expressed in adult mouse whole brain. Blue arrows show both FAM171B splice forms detected at 92kDa and 48kDa from adult mouse brain extract. The primary Ab was diluted (1:100).

However, to ensure the primary Ab bound specifically to FAM171B (but not other proteins in the brain) we performed both negative and positive controls. In the negative control (peptide block), the primary Ab was pre-incubated in peptide prior to probing for FAM171B. Incubating the primary Ab in the peptide ensures the primary Ab-binding sites are blocked. Hence, completely blocked primary Ab should not yield bands at the predicted molecular weights. Our results strongly suggest that our primary Ab (Novus) does not significantly detect proteins other than FAM171B in mouse brain (Figure 2B). Furthermore, we performed positive control experiments using human embryonic kidney (HEK-293) cell lines transfected with a FAM171B-green fluorescence protein (GFP) fusion protein. HEK cells expressing FAM171B-GFP should yield a band of ~120 kDa, and indeed we observed a strong immunostain at this predicted molecular weight (Figure 2C). Together, negative and positive control experiments strongly suggest that the Novus primary Ab recognizes FAM171B and is quite specific.

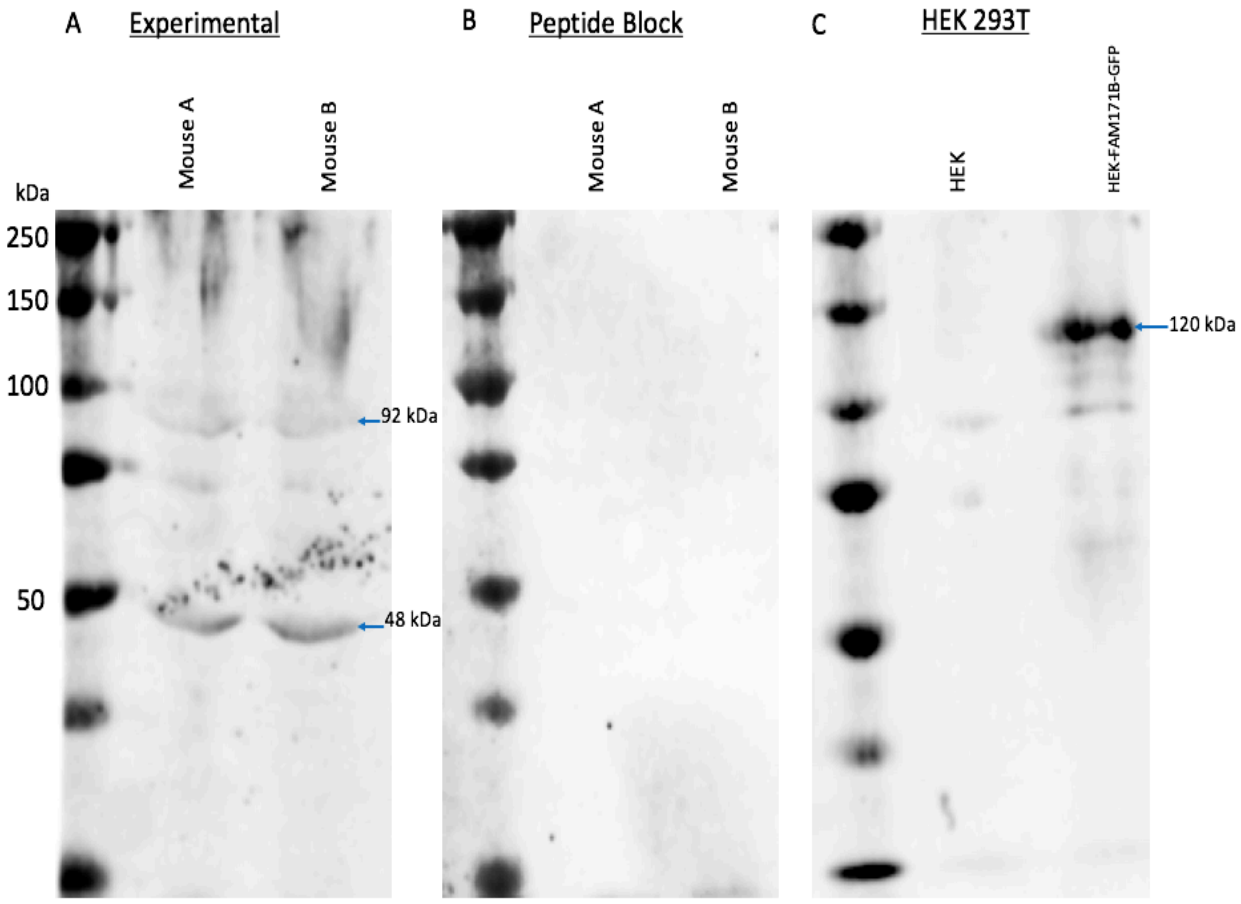

Figure 2. FAM171B negative and positive control. Immunoblots show the position of the molecular weight markers (kDa) indicated in the left. The experimental blot indicates the predominant isoform being the 48kDa (A). The peptide block did not show any cross-reactivity of antibody to proteins other than FAM171B (B). HEK transfected with FAM171B-GFP indicate a dominant band at the predicted molecular weight of 120kDa, not detected in the untransfected lane (C). The primary Ab diluted (1:1000).

With confidence in our primary Ab, we investigated the expression of FAM171B in mouse brains across all age groups used in our study. Our results reveal that FAM171B is expressed throughout post-natal development, with predominant isoforms of 92kDa

and 48kDa (Figure 3). Interestingly, however, the immunoreactive intensity of the 92kDa isoform decreased significantly from P7 to 6M. In contrast, the 48kDa isoform remained constant throughout all ages (Figure 3). Furthermore, the Ab labeled an additional band ~75 kDa in P7 that disappeared in adult mice.

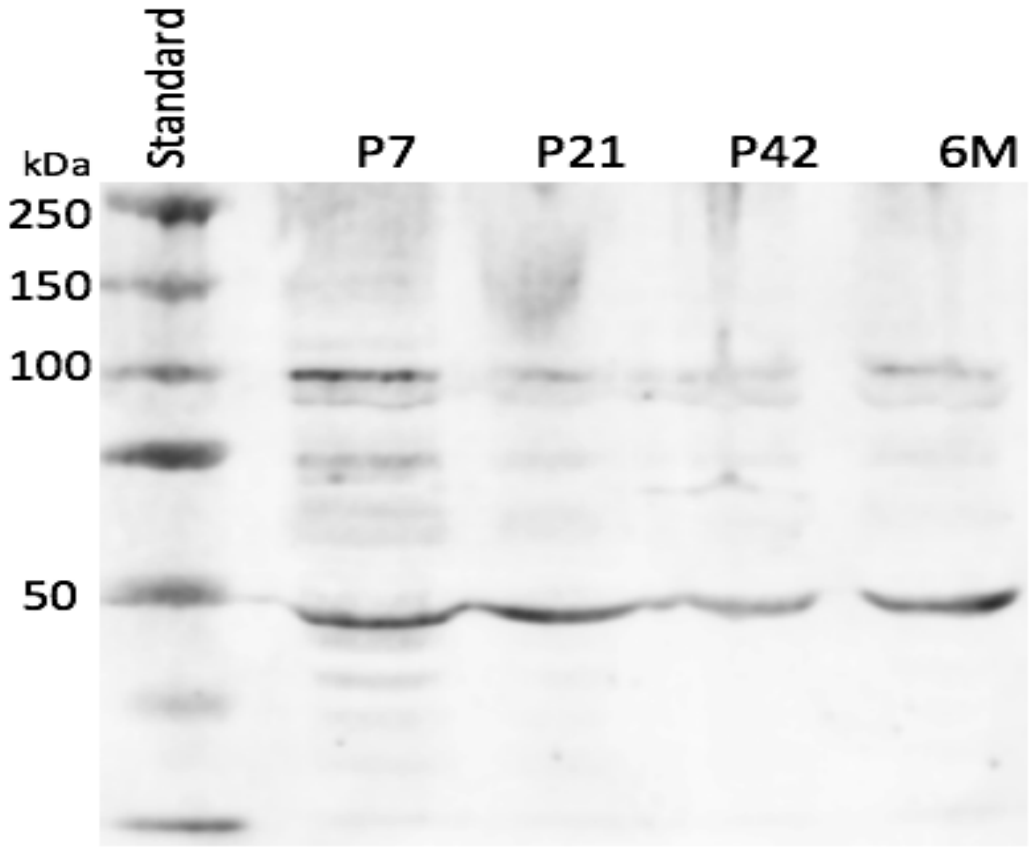

Figure 3. FAM171B is expressed in mouse whole brain across all ages. Immunoreactive bands were detected at 92kDa and 48kDa from postnatal 7, 21, 42-day, and 6-month.

We also quantified the level of FAM171B protein in each age group. Immunoreactive bands on the western blots were analyzed by IBM SPSS statistics, and univariate ANOVA was used to determine statistical differences between age groups

(Figure 4A). In addition, individual splice-forms were analyzed (Figure 4B). Although our results show a gradual decrease in FAM171B expression as mice become adults, this trend did not reach significance.

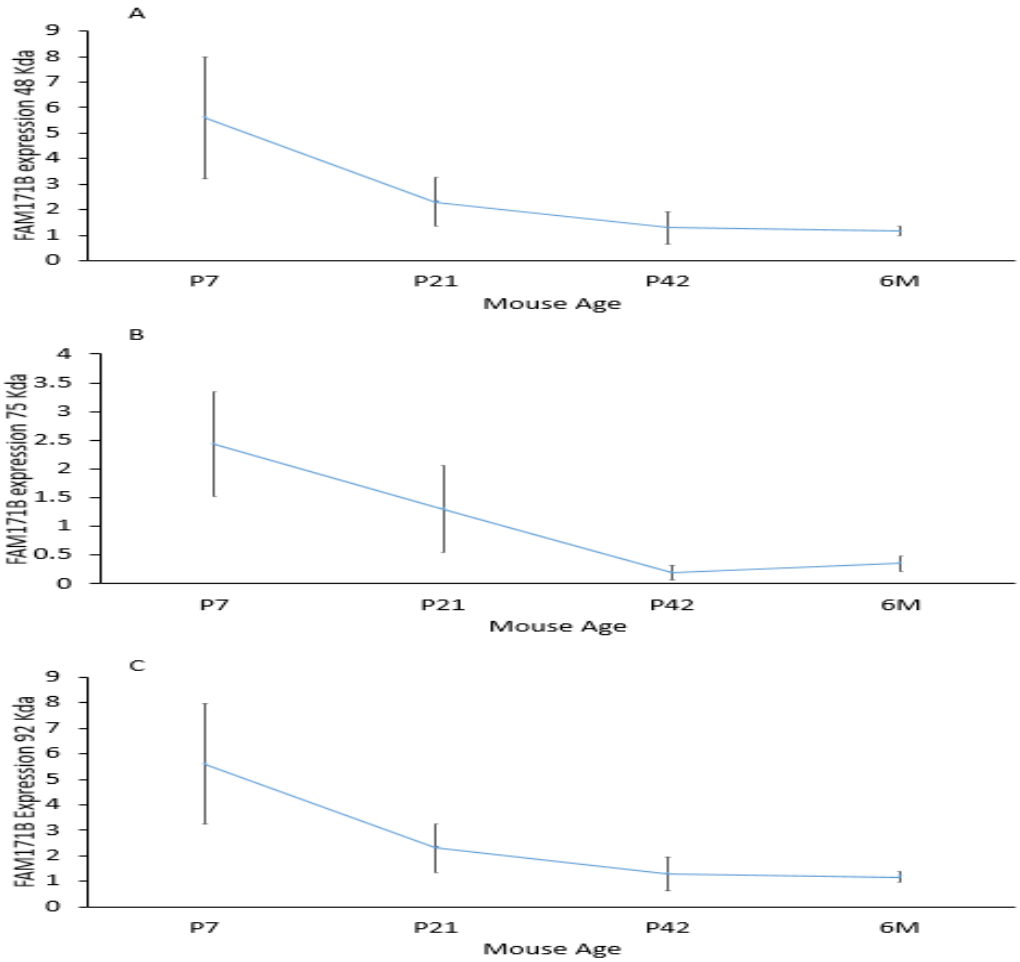

Figure 4. FAM171B age quantification. The level of FAM171B expression was highest in P7 and gradually decreased as mice became adults. Panel A shows level of protein expression from the 48kDa isoform (N=3) with univariate ANOVA analysis ($F_{3,12}$=2.47, P=0.137). Panel B shows univariate ANOVA analysis of the 75 kDa isoform ($F_{3,12}$=2.96, P=0.098). Panel C shows univariate ANOVA analysis of the 92 kDa isoform ($F_{3,12}$=3.01, P=0.095).

Furthermore, using western blotting we also examined individual brain regions for FAM171B protein expression. Various brain regions were isolated, and each individual region was probed for FAM171B expression (Figure 5). Results from these biochemical assays suggest that FAM171B is widely expressed throughout the brain, with the predominant splice-form being the 48kD species.

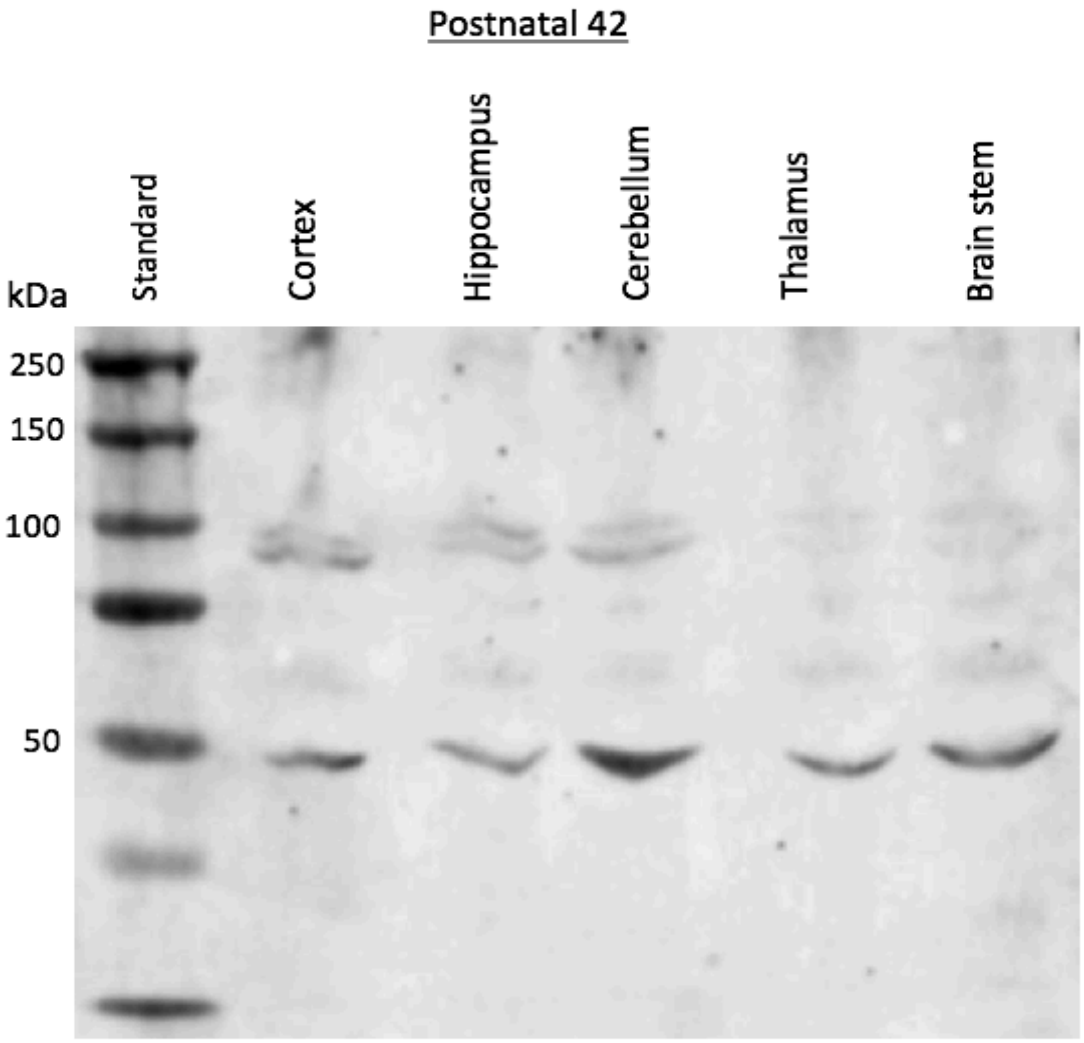

Figure 5. FAM171B expression in different mouse brain regions. Fractionated brain regions were probed for FAM171B, and immunoreactive bands were detected at 92kDa and 48kDa throughout the brain.

To further establish where FAM171B protein localizes within mouse brain, immunohistochemical assays were also performed. These studies clearly indicate the presence of FAM171B protein in many regions of mouse brain (Figure 6), and corroborate nicely our biochemical assays.

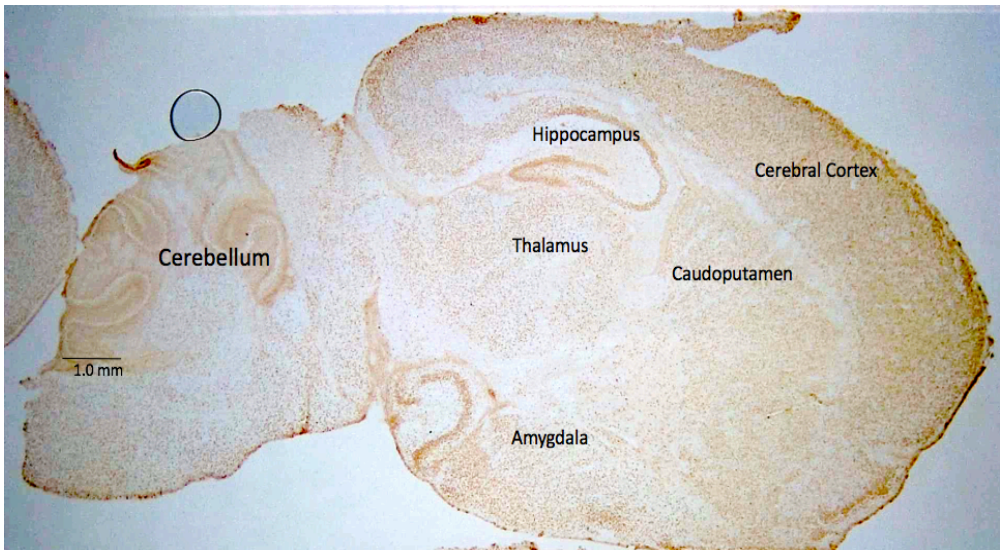

Figure 6. Whole brain section. IHC sections were photographed by dissecting microscope. Cells expressing FAM171B are stained brown. Magnification 10x.

Furthermore, these data complement nicely FAM171B mRNA expression distribution found in previous *in situ* hybridization studies (Figure 7).

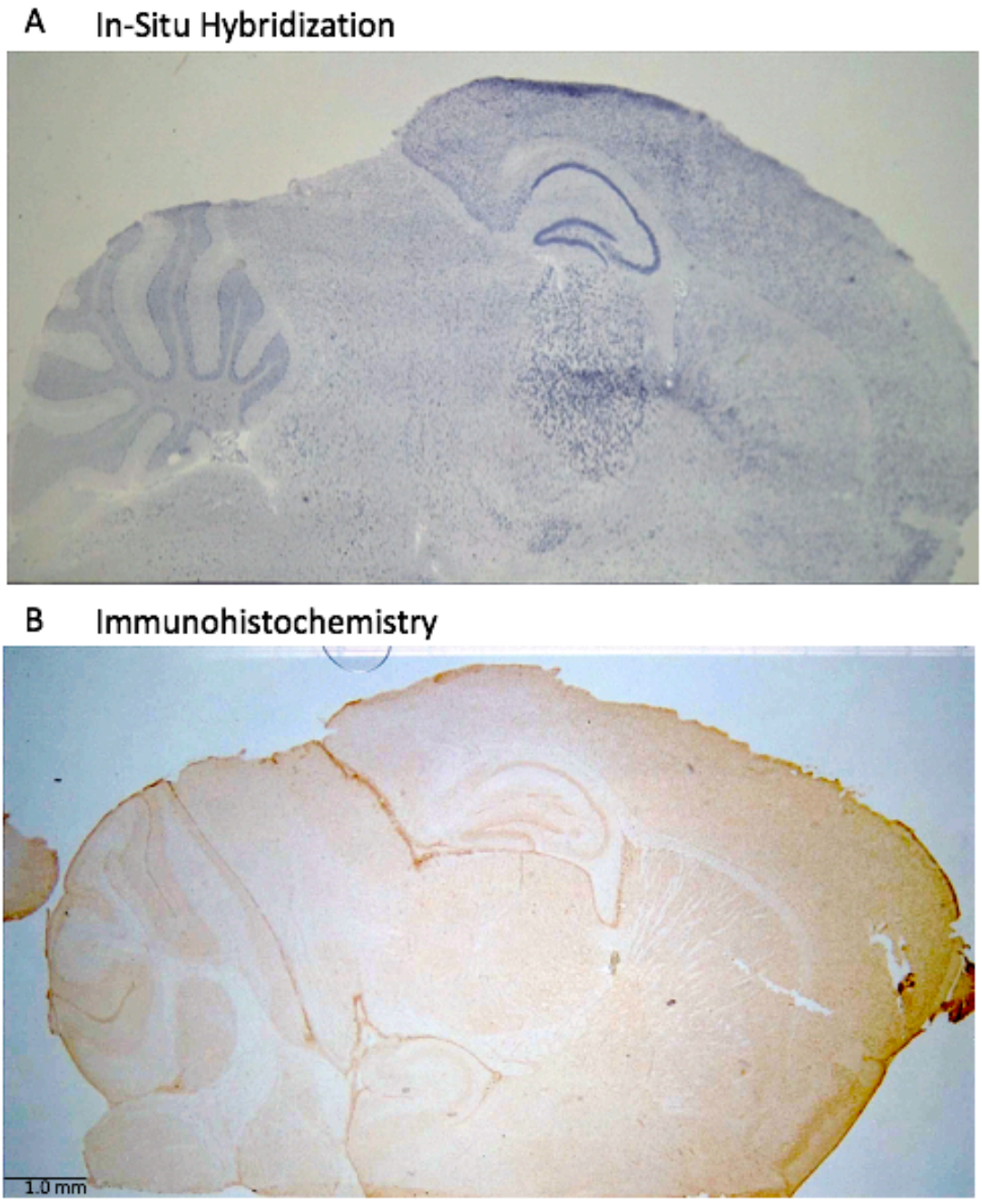

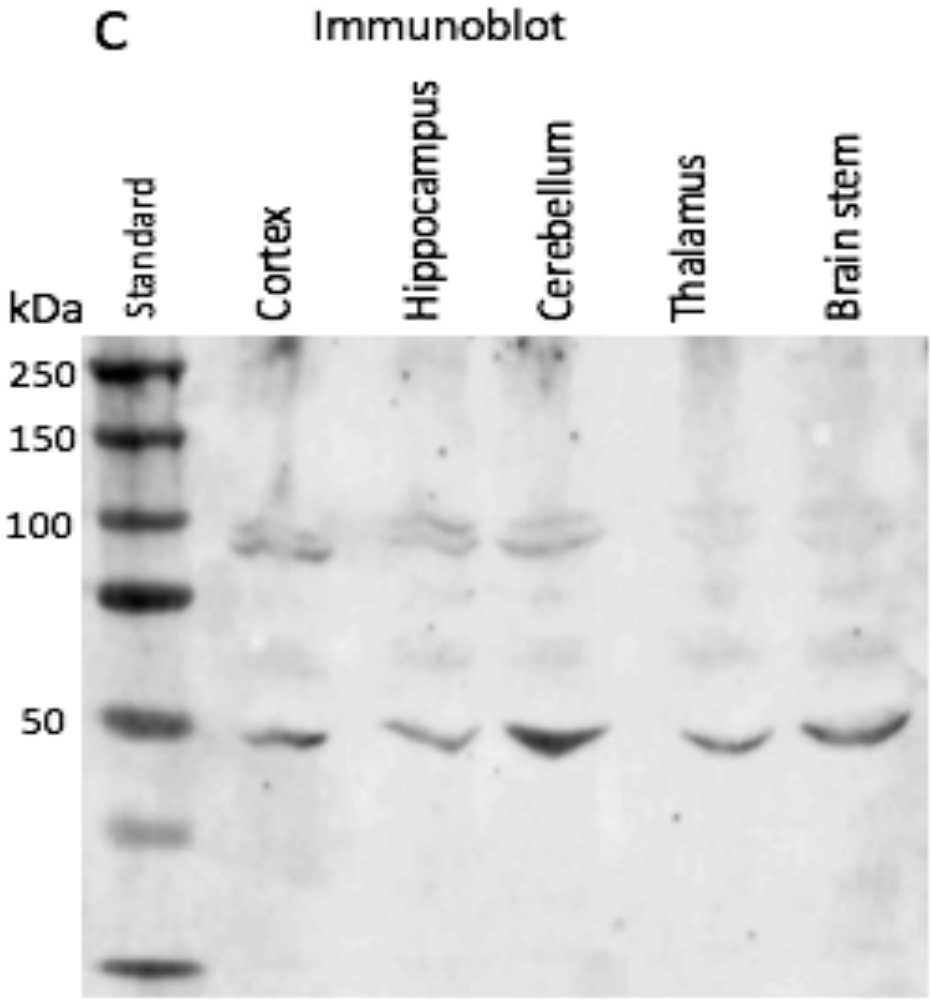

Figure 7. FAM171B expression using different assays. Widespread expression of FAM171B in the whole brain was observed using three different techniques. Microphotograph from in-situ hybridization and immunohistochemical analyses showed FAM171B widely expressed throughout the brain (A and B). Immunoblot analysis also shows FAM171B is expressed throughout the brain (C).

Such widespread expression of FAM171B from the whole brain sections raised concern whether the brown stain observed for FAM171B is a false positive as result from secondary Ab binding to tissue sections. Therefore, negative control experiments (without primary Ab) were performed to eliminate the possibility of nonspecific binding (Figure 8). Our results strongly suggest that our secondary Ab did not bind directly to the tissue.

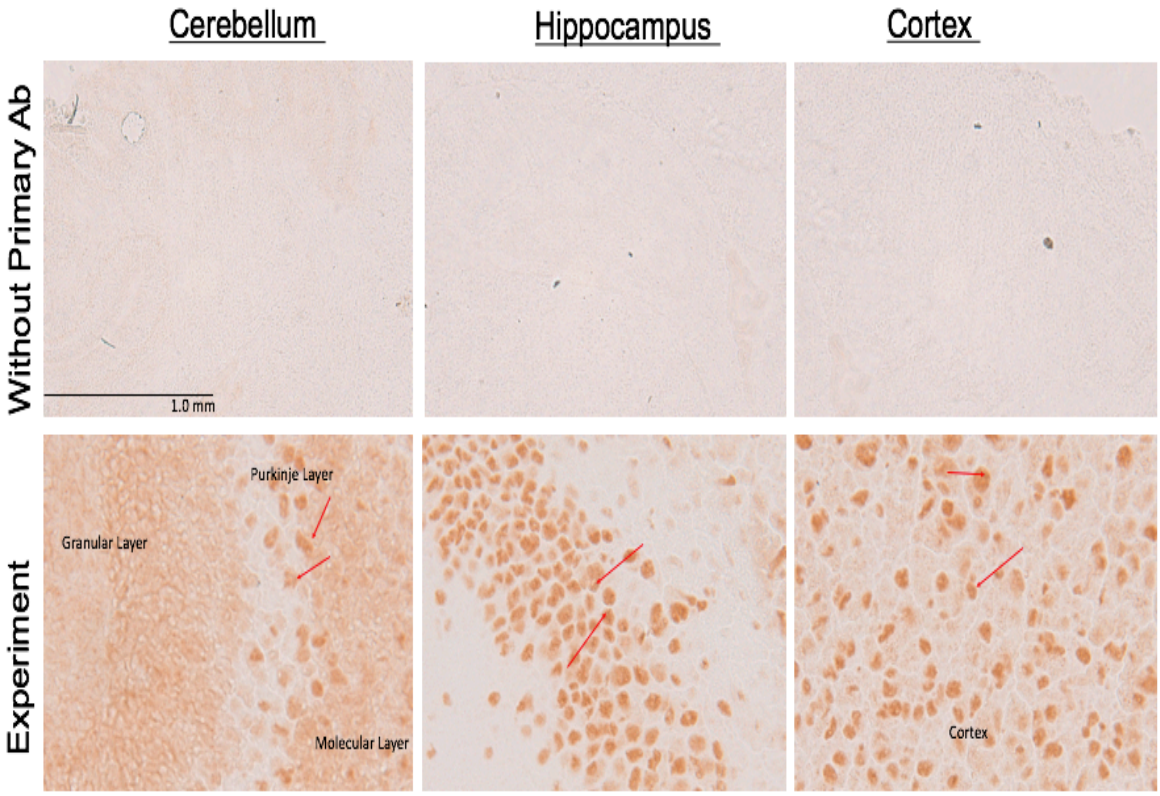

Figure 8. Negative control without primary antibody. Microphotograph from three major brain regions including the cerebellum, hippocampus, and cortex. Red arrows indicate cells expressing FAM171B protein. Negative control sections, not exposed to primary Ab, yield no stain.

Furthermore, we also performed peptide block experiments where the primary Ab-binding sites were blocked with peptide prior to IHC. As predicted, peptide block sections did not display immunostain, although experimental sections also displayed a modest decrease in staining (Figure 9).

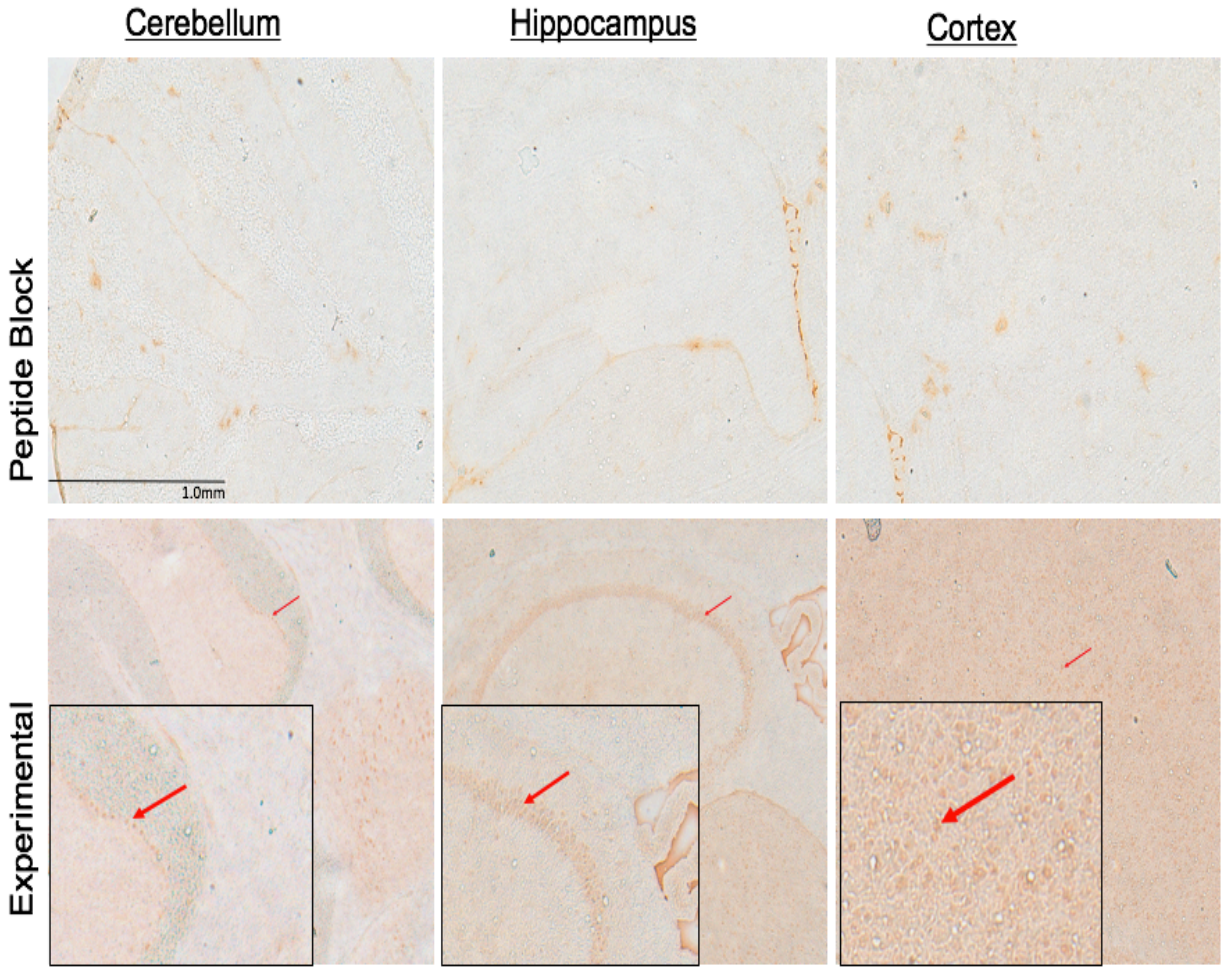

Figure 9. Peptide block control. Microphotograph from three major brain regions including the cerebellum, hippocampus, and cortex. Red arrows indicate cells expressing FAM171B protein. Peptide block control sections yielded little immunostain. Magnification 5x (Close up view in black box).

FAM171B immunohistochemical staining was qualitatively analyzed by observing the intensity and relative number of cells stained in each major brain region (Table 3). We found widespread expression of FAM171B in many brain regions of mice. Importantly, however, not all regions express it. For example, the corpus collosum white matter tract does not express FAM171B (Figure 7, Table 3).

Table 3. Qualitative analysis of FAM171B expression. Brain regions of mice across all ages were examined by light microscopy, and intensity of stain indicated by strong (+++), moderate (++), little (+), and no staining (-).

Brain Structures	P7	P21	P42	6M
Hippocampus	+++	+++	+++	++
Caudate	+++	+++	+++	++
Cerebellum	+++	++	++	+
Thalamus	+++	++	++	++
Corpus Callosum	-	-	-	-
Cortex	+++	+++	+++	++

Although FAM171B is expressed throughout the brain, we were intrigued by the pronounced expression in several specific brain regions including the hippocampus, cerebellum and cortex. In the hippocampus, FAM171B immunostain was intense across all ages (Figure 10).

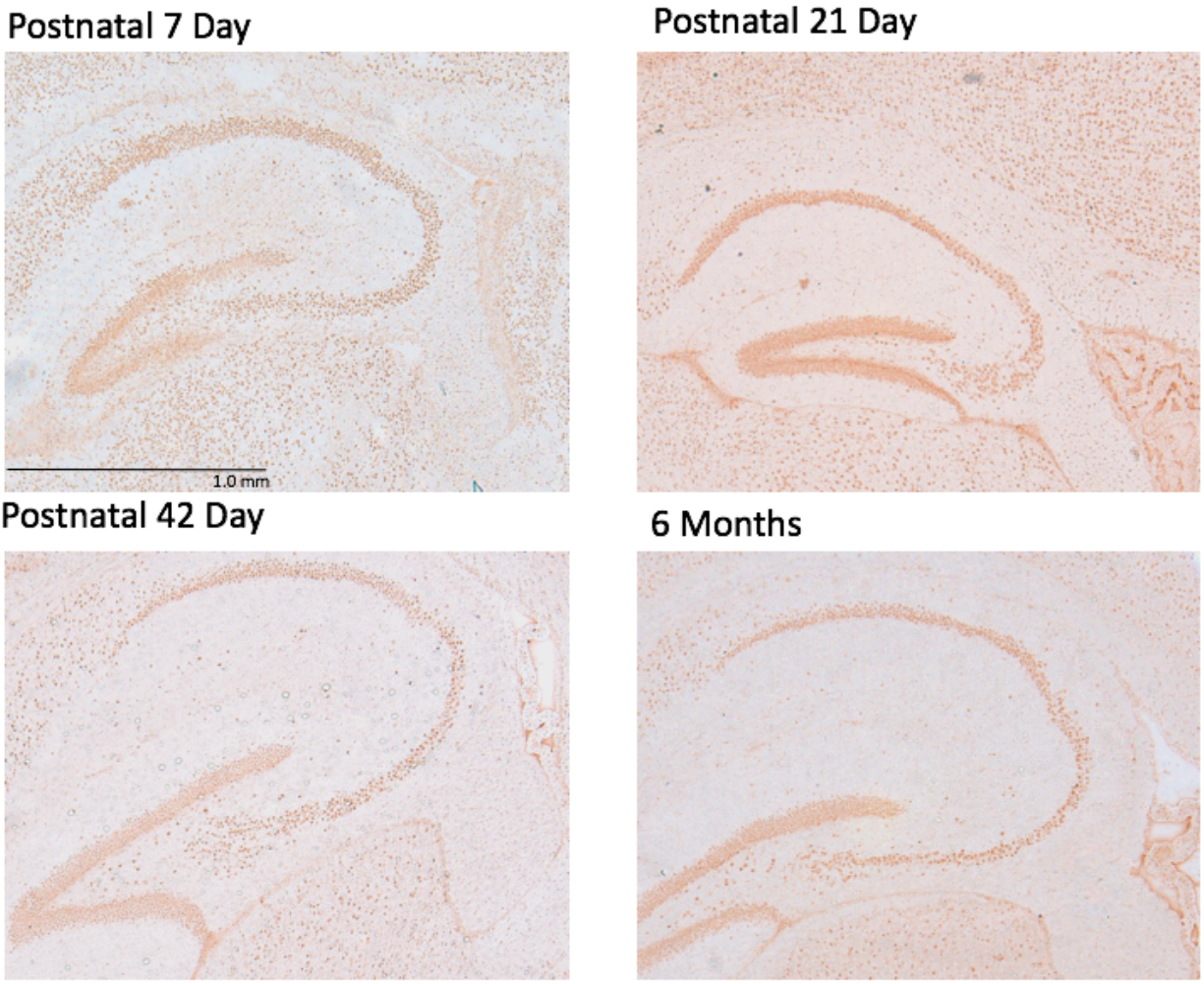

Figure 10. FAM171B is expressed in the hippocampus across all ages. Significant cellular stain was observed in both dentate gyrus and Ammons horn of the hippocampus. Magnification 5x.

Similarly, immunostain intensity was also strong in cells of the cortex throughout all age groups (Figure 11).

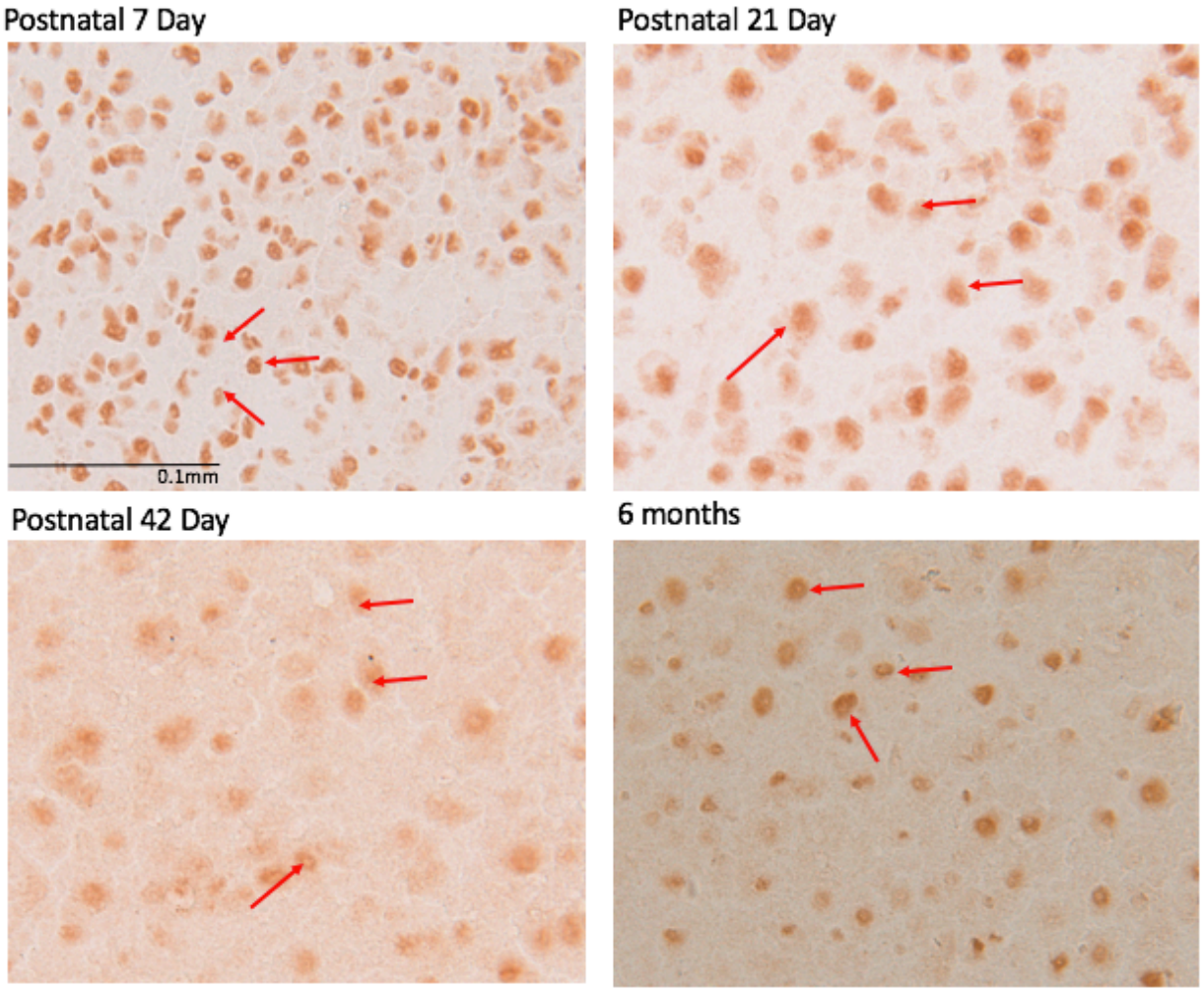

Figure 11. FAM171B expression in the cerebral cortex across all ages. Red arrows indicate cells expressing FAM171B protein. Magnification 40x.

In contrast, the immunostaining decreased somewhat in the cerebellum as mice aged, particularly in cerebellar molecular layer cells. Interestingly, similar findings were also observed in previous *in-situ* hybridization experiments (Figure 12).

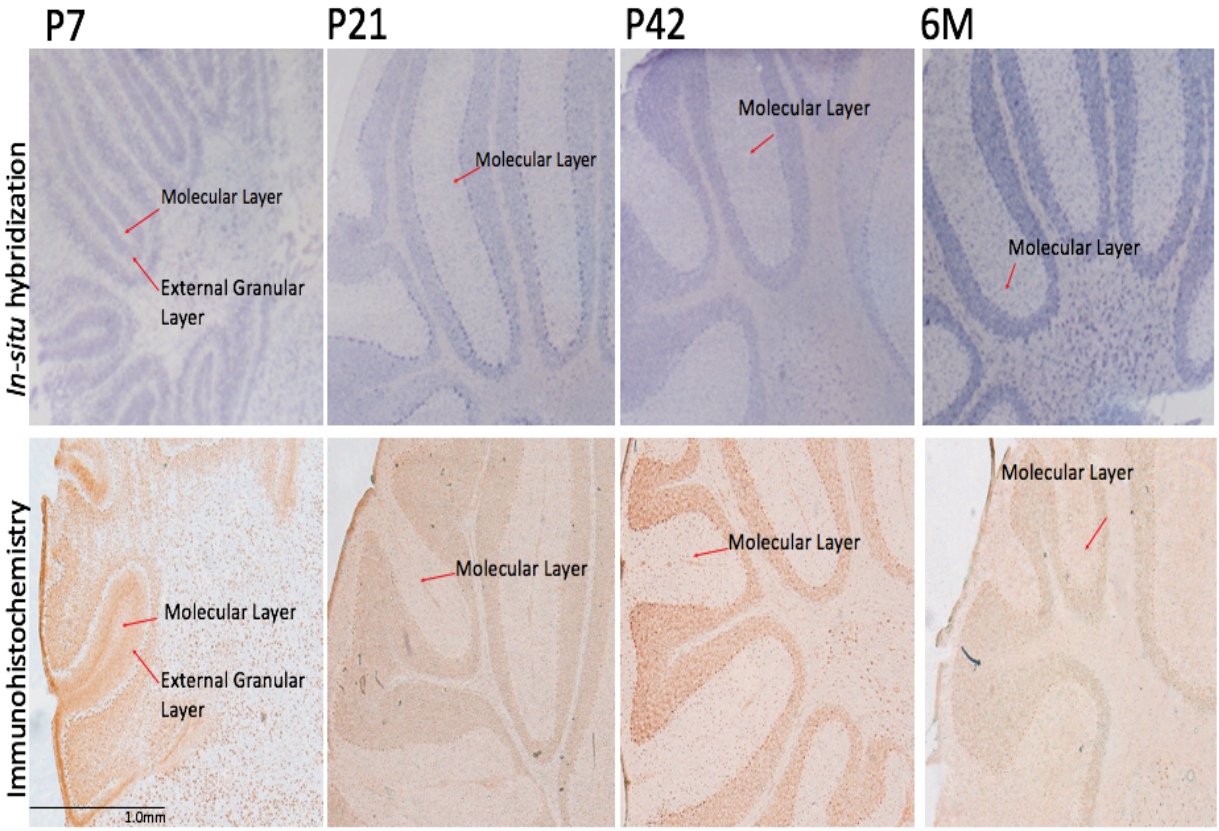

Figure 12. Molecular layer pattern in the Cerebellum. *In-situ* hybridization and IHC microphotographs of the cerebellum. FAM171B expression patterns shown in red arrows. Brown and purple color stain indicates FAM171B expression. FAM171B expression in the granular layer and Purkinje cell layers remains robust.

At a higher magnification, the staining from cerebellum of P7 appears different compared to the other age groups. Specifically, the immunostain from P7 molecular layer was much stronger than the other age groups. This phenomenon was also found using *in-situ* hybridization (Figure 13).

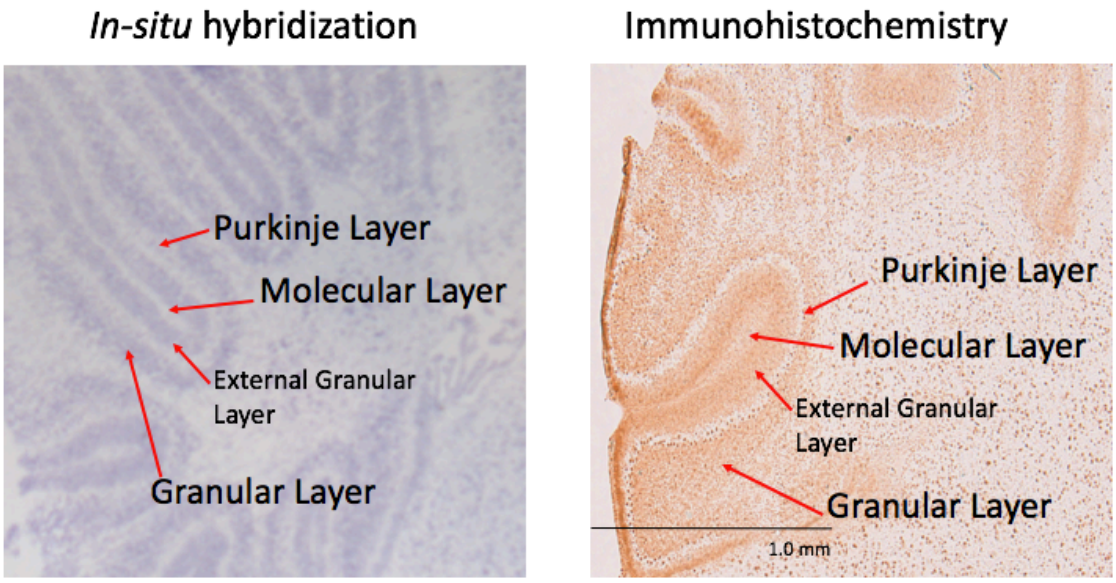

Figure 13. Cerebellum layers of P7. In-situ hybridization and immunohistochemical stains from Postnatal 7-day (P7). The brown and purple stain indicates FAM171B expression. Red arrows point to different layers in the cerebellum. Stains are strong in all three cerebellar layers of P7 mice.

In addition, the pattern of cerebellar Purkinje's cells in P7 was also different compared to other age groups. In adult mice, the Purkinje's cells were far apart from one another, and lined up in a single row. In contrast, the Purkinje cells were close to one another and somewhat disorganized in the cerebellum of P7 (Figure 14).

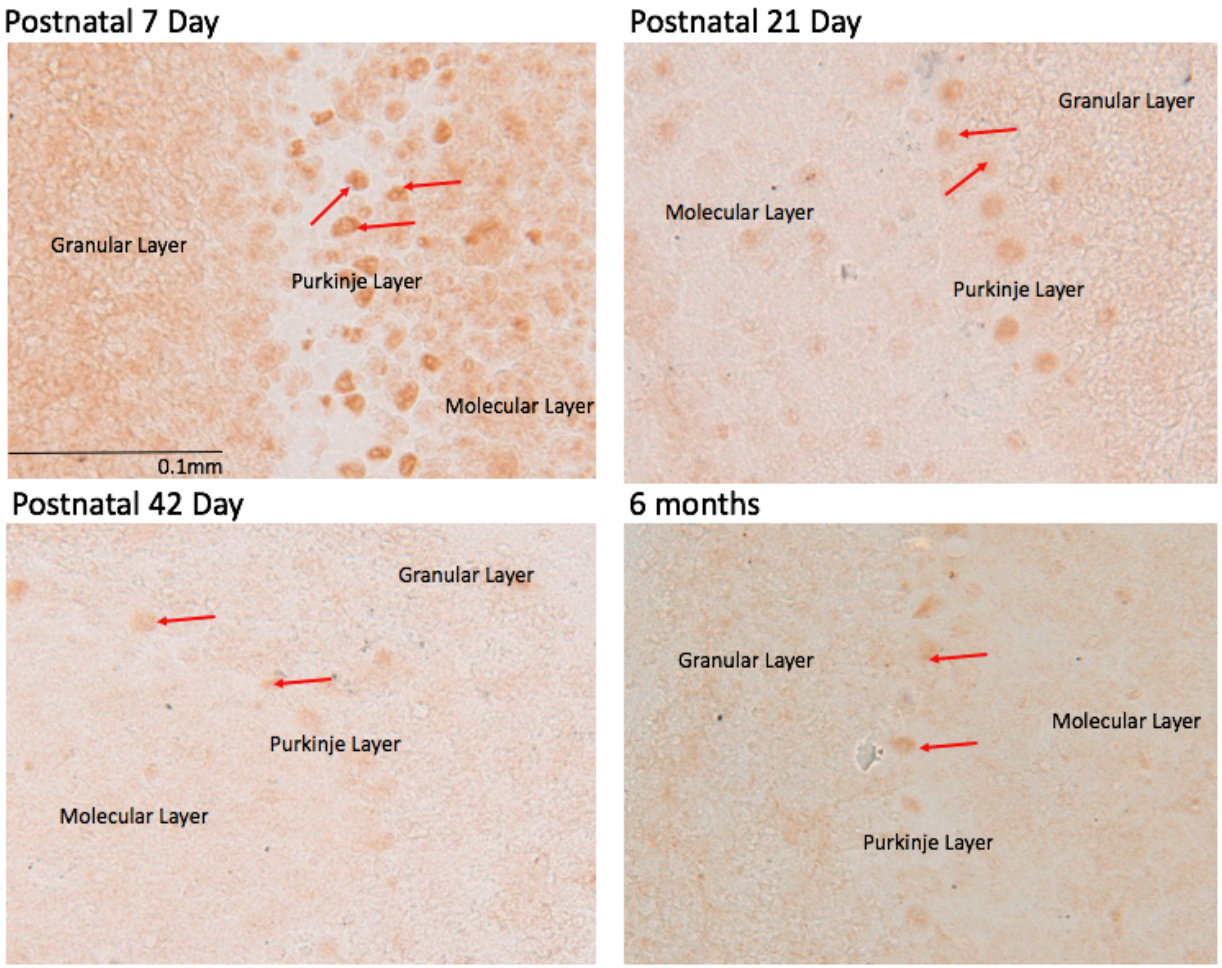

Figure 14 Purkinje cells of the cerebellum. Purkinje cells indicated by red arrows. The Purkinje cells were neighboring to one another in postnatal 7 days. In contrast, the Purkinje cells were spread out and form a single line in postnatal 42 and 6 months. Magnification 40x.

Lastly, the microphotographs reveal that the IHC stains were predominantly spherical in shape with defined border. The stain was also deposited centrally in one area of the cell, with less intense staining peripherally (Figure 15). However, where FAM171B specifically localizes within cells cannot be confirmed in this study.

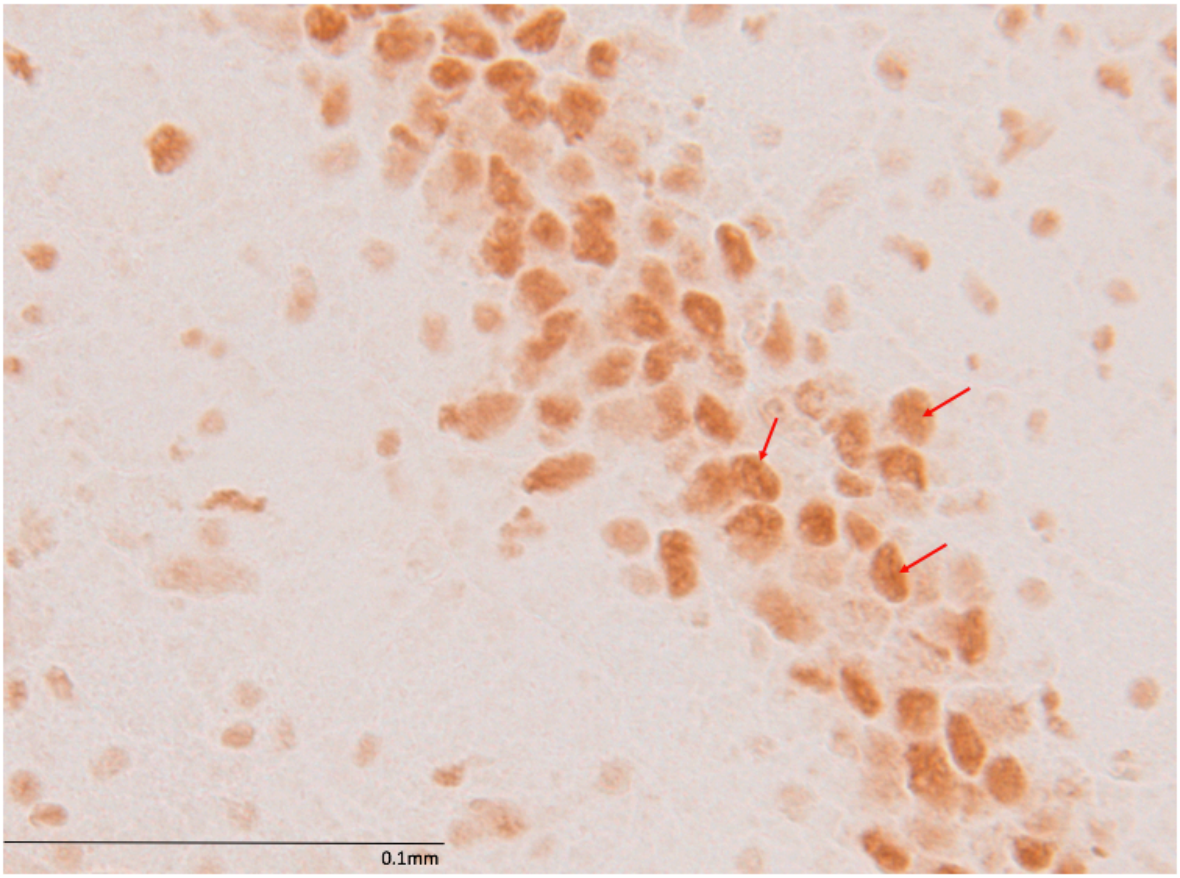

Figure 15 FAM171B expression in cortical cells. Red arrow indicates the immunostain of cells expressing FAM171B protein. A strong oval-shaped immunostain predominates in most cells. Magnification 40x.

Discussion

FAM171B is an uncharacterized novel polyQ protein that contains fourteen glutamine repeats in its reported primary amino acid sequence. Previous studies have shown that abnormally long polyQ repeats in other proteins results in severe neurodegeneration. Therefore, (if prone to expansion mutation) FAM171B might also be eventually linked to polyQ disease. Previous studies in our lab using *in-situ* hybridization suggest that FAM171B mRNA is widely expressed in the mouse brain. In this present investigation, we performed both immunoblot and immunohistochemical (IHC) analyses to confirm FAM171B protein presence and distribution in the brain. Our results strongly suggest that FAM171B protein is indeed expressed in the brain, corroborating our previous *in-situ* hybridization mRNA studies.

Western blotting of adult whole brain and isolated brain sub-regions show specific and prominent bands near 48kD and 92kD- matching nicely the predicted molecular weights of the two putative FAM171B mRNA splice forms (Figures 2,3). This data strongly argues that FAM171B is robustly expressed in mouse brain. Interestingly, immunoblot experiments do show immunoreactive bands near 75kDa in young mice that diminish in intensity as the mouse matures (Figure 3). One possible explanation for this occurrence is posttranslational processing events such as: proteolytic cleavage, phosphorylation, or glycosylation that may affect migration status of FAM171B on SDS/PAGE gels (see Table 2). An alternative explanation for the presence of “extra” bands observed in the western blot of P7 mouse brain is the possibility of non-specific binding of our primary antibody to a protein other than FAM171B. However, two pieces

of evidence strongly argue that our primary Ab does specifically detect our target protein. First, our positive control experiment (transfected FAM171B/GFP into HEK cells) shows that our Ab is absolutely able to detect FAM171B; since there is very little banding in the HEK alone lysate and a robust band near 120kD that matches the predicted molecular weight of our FAM171B fusion protein (Figure 2). Second, our peptide block experiment demonstrates that our primary Ab detects very little else besides the epitope it was raised against (Figure 2). Thus, the overall data suggests that our Ab does specifically detect FAM171B, and the presence of extra bands near 75kD in P7 mice is most likely due to posttranslational processing events.

Our IHC analysis also suggests widespread expression of FAM171B in brain (Figure 6). Furthermore, negative control (without primary Ab) experiments (Figure 8) suggest endogenous cross reactivity was completely blocked and the secondary Ab did not itself bind nonspecifically to the target tissue- giving a false positive signal. It is unclear whether the immunostain we observe is exclusively neuronal or whether FAM171B is also expressed in supporting glial cells. However, the strong immunostain observed in cerebellar Purkinje cells suggests that FAM171B is clearly expressed in certain neuronal populations (Figure 14). The most consistent and robust expression was observed in the hippocampus, cerebellum, and cortex (Figure 8). Importantly, this expression pattern matches nicely to our previous *in situ* hybridization results (Figures 7,12,13). Indeed, the combination of immunoblot, *in situ* hybridization, and IHC results all lead to the conclusion that FAM171B is robustly and widely expressed in developing and adult mouse brain.

In the cerebellum, both immunohistochemical and in-situ hybridization assay reveals a high level of FAM171B immunostain in postnatal 7-day that gradually decreases in certain cell layers as mice become adults (Figure 12). Specifically, P7 mice show intense immunostaining in the external granular layer (EGL), that diminishes in older ages (Table 3; Figure 12). It is possible that FAM171B may be synthesized differently at P7 as neurons continue to proliferate, differentiate, mature and migrate during early developmental stages (Stiles, 2010). Interestingly, our western blot finding of an "extra 75kDa band" correlates with this, and may help explain the immunostaining observed in the cerebellar EGL in P7 mice that is lacking in older ages (Figure 12). In P7 mice, FAM171B might be involved in cellular processes that aid neuronal development, and therefore specific alternative splice forms may be needed to accomplish such tasks. In contrast, as the animals mature perhaps only the predominant FAM171B 92kDa and 48kDa splice forms are necessary to maintain adult neuron survival. Also, during early brain development, neurons, glia, neuro-processes and synapses overproduced during prenatal age decrease and sometimes migrate as the mice mature into adulthood (Stile, 2010). This also might help explain the decrease in cerebellar immunostain we observe, particularly in the EGL, as mice develop into adults. As mice become adults, all forms of FAM171B may simply be less significant to certain molecular layer cells.

Structurally, the cerebellum has three distinct regions including the molecular, granular, and Purkinje cell layers. Of these layers, the molecular layer lies outermost. This layer contains basket and stellate cells that tightly synapse with Purkinje cell dendrites (*Wang*, 2002). Residing in the middle cerebellar layer are the Purkinje cells,

with their extensive dendritic trees that branch profusely and make synaptic contact with the molecular layer. Purkinje cells use GABA neurotransmitter to exert inhibitory effects on their downstream targets. Finally, the innermost cerebellar layer contains numerous granular cells that exert excitatory effects on their targets (Marr, 1969). Since it is expressed early in development, our data suggests FAM171B may play a role during formation of external granular layer cells. For example, FAM171B might help regulate the expression of gene products that initiate synapse formation during early development. Whether FAM171B serves as a transcription factor or transcription associated protein remains to be determined.

Since a number of polyQ diseases affect the cerebellum (such as SCA1, SCA2, SCA3, SCA6, SCA7), and FAM171B is significantly in this region of the brain (including Purkinje cells) our data predict that expansion mutation of the FAM171B polyQ tract may lead to a Spinocerebellar ataxia- like phenotype. Cerebellar diseases are typically characterized by poor motor coordination. For example, overexpression of mutant SCA3 decreased cerebellar Purkinje cell numbers resulting in severe cerebellar atrophy and ataxia (Paulson et al., 1997). In this regard, it would be interesting to create a similar transgenic mouse that expresses “expanded polyQ” lengths of FAM171B, and observe for phenotypic characteristics described above.

Our results show that the cerebral cortex also robustly expresses FAM171B, suggesting it may play a role in this region as well (Figure 11). The cerebral cortex is considered the “central processor” of the brain because it is responsible for: language, planning and organizing, as well as intelligence and personality determination (Bailey,

2017). Structurally, the cortex is the outermost anterior brain region with abundant folds called gyri. Folding allows for additional surface area and consequent increased brain function capacity. The cerebral cortex contains a large number of neuronal and glial cell bodies, as well as their dendritic and axonal projections (Kandel, 2000).

At the cellular and circuit level, the cerebral cortex is subdivided into various functional areas including sensory, motor, and higher order cognitive regions. Therefore, neuronal cell loss in the cortex may result in progressive deterioration of motor and cognitive function. For example, prominent cell death occurs in the neostriatum and cortex in adult onset HD (Francis, 2007). As a result, affected HD individuals show jerky voluntary movements (chorea), irritability, depression and other mood alterations (Harper, 1991). As the disease progresses the chorea movements become prominent, and abilities such as walking, speaking, and swallowing progressively deteriorate (Thompson et al., 1998). Based on its localization in brain, it may be predicted that expansion mutation in FAM171B may also lead to similar phenotypes.

FAM171B is also expressed in the hippocampus of mice, suggesting that it may normally function in memory formation- as the hippocampus plays a major role in this regard (Columbo, 2000). Structurally, the hippocampus resembles a horseshoe shape, and is a paired structure located on each side of the brain (Amaral, 2007). Damage to the hippocampus significantly decreases the capacity to form new memories (Di Gennaro, 2006). Indeed, *in vivo* studies of long-term social memories demonstrate that the hippocampus is significantly involved in memory consolidation and social recognition (Matthies, 1989; van Wimersa Greidanus, 1996). Interestingly, in HD individual neuronal

density significantly decreases in the CA1 area of the hippocampus resulting in memory impairment (Spargo, 1993). Therefore, we predict that mice carrying mutant FAM171B, (or perhaps even knockout mice) might be unable to consolidate memory or exhibit cognitive impairment.

Although FAM171B's cellular function in these areas remains unknown, knowledge of basic neuroanatomy and from polyQ disease pathologies enable us to predict roles in which FAM171B may play in these areas. However, to confirm function, we would need to create and observe mice carrying either wildtype or mutant FAM171B gene for clinical pathology signs and symptoms indicative of polyQ disease.

It will also be interesting to determine where FAM171B resides and functions within cells. Aberrant polyQ proteins are found within various cellular compartments (Table 1). For example, in spinal bulbar muscular atrophy androgen receptor (AR) polyQ expansion results in neurodegeneration and SBMA (Simanainen et al., 2011). In the cytoplasm, normal AR passes signals from androgens to target genes by interacting with coregulatory proteins in the cytoplasm and specific response-elements in the DNA. Androgens are important in the development and function of numerous tissues including: skeletal muscle, bone marrow, hair follicles, male reproductive system, and brain (Bagatell, 1996). Thus, mutations in the AR prevents androgen binding and proper signaling of downstream gene expression. Indeed, partial to complete androgen insensitivity and infertility result from AR mutation. (Gottlieb, 2001; De Bellis 1914).

Although our present study cannot determine whether FAM171B is exclusively expressed in the nucleus, our data does show predominant oval-shaped immunostaining

with a well-defined border (Figure 15). Thus, FAM171B may function in neuronal nuclei. However, further studies such as co-immunofluorescence coupled with confocal microscopy will be required to definitively confirm intracellular localization of FAM171B. Understanding intracellular localization of FAM171B will greatly aid us in predicting its function within neurons. Additionally, protein- protein interaction studies should shed light on FAM171B's role in cellular processes. Indeed, these studies are currently ongoing in our lab- using techniques such as immunofluorescence and co-immunoprecipitation.

As a novel polyQ protein that is expressed in the brain, our observations suggest that FAM171B should be considered a candidate gene for as yet molecularly uncharacterized neurodegenerative diseases. Further efforts in our lab include using bioinformatic tools to search for diseases that map near the FAM171B locus (2q32.1). If a disease gene is eventually linked near this chromosomal region, one could use PCR and sequencing methodologies to assay FAM171B CAG repeat tract length in normal and disease individuals. We would expect to find increased repeat tract lengths in affected individuals only- if mutations in FAM171B cause the disease. It will be interesting to see if FAM171B is ever linked to a disease in this way. Regardless, basic biological studies of FAM171B (similar to these current experiments) will shed light on its normal function within cells of the brain.

References:

1. Agnieszka F., and Wlodzimierz J.K. (2014). Oligonucleotide-based strategies to combat polyglutamine diseases. Nucleic Acids Research 42:6787-6810.

2. Amaral, D, Lavenex, P. (2007). Hippocampal neuroanatomy. New York: Oxford University Press. p. 37

3. Bagatell, C.J. and Bremner, W.J. (1996) . N.Engl.J.Med 334:707-714.

4. Bailey, R. (2017) Anatomy of the Brain- Cerebral Cortex. *Thoughtco*.

5. Bauer, P. O. and Nukina, N. (2009). The pathogenic mechanisms of polyglutamine diseases and current therapeutic strategies. J. Neurochem. 110:1737–1765

6. Bradford, J.W., Li, S., and Li X.J. (2010) Polyglutamine toxicity in non-neuronal cells. Cell Res. 20:400-407.

7. Colombo, M., Broadbent, N.. (2000). Is the avian hippocampus a functional homologue of the mammalian hippocampus?. Neuroscience and Biobehavioral Reviews. **24**: 465–84.

8. De Bellis, A., Quigley, C. A., Marschke, K. B., El-Awady, M. K., Lane, M. V., Smith, E. P., French, F. S. (1994). Characterization of mutant androgen receptors causing partial androgen insensitivity syndrome. The Journal of Clinical Endocrinology & Metabolism, 78(3), 513–522.

9. Di Gennaro, G., Grammaldo, L.G., Quarato, P.P., Esposito, V., Mascia, A., Sparano, A., Meldolesi, G.N., Picardi, A. (2006). Severe amnesia following bilateral medial temporal lobe damage occurring on two distinct occasions. Neurological Sciences. **27**: 129–33

10. Duennwald, M. L., Jagadish, S., Muchowski, P. J., and Lindquist S. (2006). Flanking sequences profoundly after polyglutamine toxicity in yeast. Proceedings of the National Academy of Sciences of the USA 103: 11045–11050.

11. Francis O.W. (2007). Huntington's disease. The lancet 369: 218-228.

12. Gacy, A.M., Goellner G.M., Juranic N., Macura S., and C.T. McMurray. (1995) Trinucleotide Repeats That Expand in Human Disease Form Hairpin Structures In Vitro. Cell. 81:533-540.

13. Goellner, G.M., Tester, D., Thibodeau, S.N., Almqvist, E., Goldberg, Y.P., Hayden, M.R., and McMurray C.T. (1997) Different Mechanisms Underlie DNA Instability in Huntington Disease and Colorectal Cancer. Am. J. Hum. Gen. 60:879-890.

14. Goellner, G.M. and M.C. Rechsteiner. (2003) Are Huntington's and Polyglutamine Based Ataxia's Proteasomal Storage Diseases? Int. J. Biochem. Cell Biol. 35(5):562-71. Review.

15. Gottlieb, B., Beitel, L. K., & Trifiro, M. A. (2001). Variable expressivity and mutation databases: the androgen receptor gene mutations database. *Human Mutation*, *17*(5), 382–388.

16. Haacke, A., Broadley, S. A., Boteva, R., Tzvetkov, N., Hartl, F. U., and Breuer, P. (2006). Proteolytic cleavage of polyglutamine-expanded ataxin-3 is critical for aggregation and sequestration of nonexpanded ataxin-3. Human Molecular Genetics 15: 555–568.

17. Harper P. S. (1991). Huntington's Disease. Philadelphia, PA: W. B. Saunders

18. Hueng-Chuen F., Li-Ing H., Ching-Shiang C., Shyi-Jou C., Giia-Sheun P., Tzu-Min C., Shinn-Zong L.,and Horng-Jyh H. (2014). Polyglutamine (PolyQ) Diseases: Genetics to Treatments *Cell Transplantation* 23: 441–458.

19. Huynh, D.P., Figueroa, K., Hoang, N. and Pulst, S.M. (2000). Nuclear localization or inclusion body formation of ataxin-2 are not necessary for SCA2 pathogenesis in mouse or human. *Nat. Genet.*, 26, 44–50.

20. Ikeda, H., Yamaguchi, M., Sugai, S., Aze, Y., Narumiya, S., and Kakizuka A. (1996). Expanded polyglutamine in theMachado-Joseph disease protein induces cell death in vitro and in vivo. Nature Genetics 13:198–202.

21. Kandel, E. R., Schwartz, J. H., Jessell, T.M. (2000). Principles of Neural Science (Fourth ed.). United State of America: McGraw-Hill p. 324

22. Kovtun, I.V., McMurray, C. (2001). Trinucleotide expansion in haploid germ cells by gap repair, Nat. Genet. 27 407–411. DNA repair. 7: 1121-1134.

23. Kovtun IV, Goellner G.M., and C.T. McMurray. (2001) Structural features of trinucleotide repeats associated with DNA expansion. Biochem Cell Biol. 79(3):325-36. Review.

24. La Spada, A.R., Wilson, E.M., Lubahn, D.B., Harding, A.E. and Fischbeck, K.H. (1991). Androgen receptor gene mutations in X-linked spinal and bulbar muscular

atrophy. Nature. 352: 77–79.

25. La Spada, A. R., Roling, D. B., Harding, A. E., Warner, C. L., Spiegel, R., Hausmanowa-Petrusewicz, I., ... & Fischbeck, K. H. (1992). Meiotic stability and genotype-phenotype correlation of the trinucleotide repeat in X-linked spinal and bulbar muscular atrophy. *Nature genetics*, *2*: 301.

26. Manley, K., Shirley, T.L., Flaherty, L., Messer, A. (1999). MSH2 deficiency prevents *in vivo* somatic instability of the CAG repeat in Huntington disease transgenic mice. Nat. Genet. 23: 471–473.

27. Margulis, B. A., Vigont, V., Lazarev, V. F., Kaznacheyeva, E. V., Guzhova, I. V. (1997–2007). Pharmacological protein targets in polyglutamine diseases: Mutant polypeptides and their interactors. FEBS Lett. 587 (13): 2013.

28. Marr, D. (1996). A theory of cerebellar cortex. Journal Physiol. Lond 202:437-470.

29. Matthies, H. (1989). In search of cellular mechanism of memory. Pro Neurobiol 32:277-349.

30. McMurray, C. (2008). Hijacking of the mismatch repair system to cause CAG expansion and cell death in neurodegenerative disease. DNA Repair 7: 1121-1134.

31. McMurray, C.T. (2010) Mechanisms of trinucleotide repeat instability during human development. Nature Reviews Genetics 11, 786–799.

32. Nguyen, D.F, Zhou, T., Shu, J., Mao, J-H. (2013). Quantifying chromogen intensity in immunohistochemistry via reciprocal intensity. Cancer Incytes 2 issue 1

33. Nucifora Jr., F.C., Sasaki, M., Peters, M.F., Huang, H., Cooper, J.K., Yamada, M., Takahashi, H., Tsuji, S., Troncoso, J., Dawson, V.L., et al. (2001). Interference by huntingtin and atrophin-1 with CBP-mediated transcription leading to cellular. 291: 2423-2428

34. Paulson, H. L., Perez, M. K, Trottier, Y., et al. (1997). Intranuclear inclusions of expanded polyglutamine protein in spinocerebellar ataxia type 3. Neuron 19: 333–344.

35. Ross, C.A. and Poirier, M.A. (2004). Protein aggregation and neurodegenerative disease. Nat. Med. 10 (supply), S10–S17.

36. Saudou, F., Finkbeiner,S., Devys, D. and Greenberg, M.E. (1998). Huntingtin acts in the nucleus to induce apoptosis but death does not correlate with the formation of intranuclear inclusions. *Cell* 95: 55–66.

37. Sharp, A.H., Love, S.J., Schilling, G., Li, S.-H., Bao, J., Wagster, M.V., Kotzuk, J.A. Steiner, J.P., Lo, A. *et al.* (1995). Widespread expression of Huntington's disease gene (IT15) protein product. Neuron 14:1065-1074.

38. Simanainen, U., Brogley, M. Gao, Y.R., Jimenez, M., Harwood, D.T., et al. (2011) Length of the human androgen receptors glutamine tract determine androgen sensitivity in vivo. Mol. Cell. Endocrinol 342:81-86.

39. Spargo, E., Everall, I. P., & Lantos, P. L. (1993). Neuronal loss in the hippocampus in Huntington's disease: a comparison with HIV infection. *Journal of Neurology, Neurosurgery, and Psychiatry*, *56*(5), 487.

40. Stiles, J., & Jernigan, T. L. (2010). The Basics of Brain Development. *Neuropsychology Review*, *20*(4), 327–348

41. Tarlac,V., Turnbull,V., Stefani,D., Kelly,L., Walsh,R. and Storey,E. (2007). Inclusion formation by ataxins -1, -2, -3, and -7. *Int. J. Neurosci.*, 117: 1289–1314.

42. The UniProt Consortium (2017). UniProt: the universal protein knowledgebase. Nucleic Acids Res. 45: D158-D169

43. Thompson P. D., Berardelli A., Rothwell J. C., Day B. L., Dick J. P., Benecke R., et al. (1988). The coexistence of bradykinesia and chorea in Huntington's disease and its implications for theories of basal ganglia control of movement. Brain 111: 223-244

44. Van Wimersma Greidanus T.B, Maigret C. (1996). The role of limbicvasopressin and oxytocin in social recognition. Brain Res 713:153–159.

45. Walker F.O. (2007) Huntington's disease. Lancet 360:218-228

46. Wang, Y.; Gupta, A; Toledo-Rodriguez, M; Wu, C. Z.; Markram, H (2002). "Anatomical, Physiological, Molecular and Circuit Properties of Nest Basket Cells in the Developing Somatosensory Cortex". Cerebral Cortex. **12** (4): 395–410

47. Williams, A.J., and Paulson, H.L. (2006). Polyglutamine neurodegenerative disease and regulation of transcription: assembling the puzzle. Genes Development 20:2183-2192.

48. Wood, E.R., Dudchenko P.A, Eichenbaum H. (1999). The global record of memory in hippocampal neuronal activity. Nature 397:613-616.

49. Xia, H., Mao, Q., Eliason S.L., Harper, S.Q, Martins, I.H., Orr, H.T., Paulson, H.L., Yang, L., Kotin R.M., and Davidson, B.L. (2004). RNAi suppresses polyglutamine-induced neurodegeneration in a model of spinocerebellar ataxia. Nat Med 8:816-820.

50. Yoo, S.Y., Pennesi, M.E., Weeber, E.J., Xu, B., Atkinson, R.,Chen, S., Armstrong, D.L., Wu, S.M., Sweatt, J.D., and Zoghbi, H.Y. (2003) SCA7 knockin mice model human SCA7 and reveal gradual accumulation of mutant ataxin-7 in neurons and abnormalities in short-term plasticity. Neuron 37: 383–401.

51. Zoghbi, H. Y.; Orr, H. T. (1999). Polyglutamine diseases: Protein cleavage and aggregation. Curr. Opin. Neurobiol. 9: 566–570

52. Zoghbi, H.Y. and Orr, H.T. (2000) Glutamine repeats and neurodegeneration. Ann. Rev. Neurosci. 23: 217–247.

53. Zühlke, C., Rless, O., Bockel, B., Lange, H., & Thies, U. (1993). Mitotic stability and meiotic variability of the (CAG) n repeat in the Huntington disease gene. *Human Molecular Genetics*, *2*(12), 2063–2067.